THE ASTROPHYSICAL JOURNAL, 434:599–613, 1994 October 20

HOT GAS IN THE INTERSTELLAR MEDIUM: A REANALYSIS OF O VI ABSORPTION DATA

R. L. SHELTON AND D. P. COX
Department of Physics, University of Wisconsin—Madison, 1150 University Avenue, Madison, WI 53706
Received 1993 June 30; accepted 1994 April 29

ABSTRACT

The *Copernicus* O^{+5} column densities toward 72 stars provide a rare and valuable tracer of $10^{5.5}$ K gas in the interstellar medium. The original analysis of the data by Jenkins provided important clues about the distribution of interstellar O^{+5} ions, but our understanding of the local interstellar medium has since grown substantially. We revisit that work, including the possibility that local hot gas may contribute a significant O^{+5} column density to most lines of sight. Our reanalysis also includes slight improvements in the statistics and was found to be reliable when tested on simulated data sets.

In the end, we come to conclusions about the distribution of interstellar O^{+5} ions that differ considerably from those of the original analysis.

1. Good fits can be found by including the entire data set.
2. The combined mean column density of the Local Bubble and its interface with the Local Cloud is roughly 1.6×10^{13} cm^{-2}.
3. We find a smaller value for the midplane volume density of O^{+5} ions outside the Local Bubble (1.3–2.1×10^{-8} cm^{-3}) than Jenkins's 2.8×10^{-8} cm^{-3} found assuming no Local Bubble.
4. The O^{+5}-bearing material beyond the Local Bubble is probably clumped into features of much larger column density than estimated by Jenkins (2–7×10^{13} O^{+5} ions cm^{-2} vs. 1×10^{13} cm^{-2}).
5. The mean line-of-sight distance between features beyond the Local Bubble is thus several times that of Jenkins (450–1300 pc vs. 165 pc).

These changes strongly influence our understanding of the phase distribution in the interstellar medium, in particular the volume occupation of the hot and warm components, and mechanisms responsible for them. Stellar wind bubbles, cloud interfaces, fountains, and supernova remnants are discussed.

With our reanalysis, some theoretical models now show promise. For example, our Local Bubble column density compares favorably with the estimated quantity of O^{+5} within the remnant of an ancient local explosion. Similarly, our mean O^{+5} column density per feature in more distant regions is like that found in models of hot interstellar bubbles from either stellar winds or ancient supernova explosions in a warm diffuse interstellar environment, suggesting that the hot gas in interstellar space may exist primarily within discrete regions of modest volume occupation rather than in a continuous and pervasive phase.

Subject headings: ISM: bubbles — ISM: general — methods: statistical — ultraviolet: ISM

1. INTRODUCTION

Almost all information on the hot gas distribution within or surrounding the Galactic disk derives from only three direct measures: the diffuse soft X-ray background at low and medium energies, the high-stage ion populations (chiefly C^{+3}, N^{+4}, and O^{+5}) observed in absorption in the UV, and the limited information so far available on the FUV and EUV emission line backgrounds. Each data set deserves careful scrutiny.

Of these measures, the O VI absorption data taken toward O and B stars during the 1970's by the *Copernicus* satellite are especially useful for three essential reasons: they were accumulated from stars to fairly large distances, sampling a much larger scale than could be studied in EUV or one-quarter keV X-ray emission; the ion samples rather high-temperature gas ($\sim 10^{5.5}$ K) with little contamination expected from photoionization; in addition, the line strengths are sufficiently great that even fairly nearby stars have detectable column densities. Star-to-star fluctuations in column density per distance can be used as a measure of the probable magnitude of individual components.

These data were presented and initially analyzed in a classic series of papers by Jenkins (1978a, b, c), including a statistical treatment of the column density fluctuations. Since that time, however, it has become increasingly clear that a sizeable region of hot gas, the Local Bubble, is present in the local interstellar medium (see review by Cox & Reynolds 1987). In fact, the existence of a local O^{+5} contribution associated with this hot gas is consistent with the nonzero intercept in the O^{+5} column density versus stellar distance relation found by Jenkins (1978c). The presence of such gas has prompted us to revise Jenkins's (1978b) fluctuation analysis.

The picture underlying the analysis assumes that the O^{+5} ions are confined to regions occupying only a small fraction of interstellar space, and that these regions are randomly distributed within the Galactic plane, with prevalence decreasing with increasing altitude.[1] On average, an encounter between a sight line and such a region contributes $\overline{N_o}$ to the observed column density, though there may be great variation about this average. We suppose the existence of a local contribution (the combined mean column density of the Local Bubble and its

[1] Our mathematical model is phrased in terms of the dominant paradigm in which regions of hot gas are scattered about in an environment of cooler gas. The mathematical analysis is also applicable to a model in which the O^{+5} resides at the interfaces between regions of cold gas that are scattered about in an environment of extremely hot gas, as long as the environmental gas is too hot to contain significant quantities of O^{+5} ($T \gtrsim 2 \times 10^6$ K).

interface with the Local Cloud) of average column density $\overline{N_{lb}}$ (again with considerable variability), along the paths to all stars more distant than the Local Bubble boundary. Finally, based on the experience of Jenkins (1978b), one must be watchful for uncommon interstellar regions of anomalously high column density that are not well described by the model. Given these assumptions about the origins of the O VI absorption, the analysis provides a quantitative measure of the goodness of fit between models with assumed parameters and the observed data. From this, one abstracts acceptable parameter ranges for the Local Bubble's mean column density, for the mean interstellar feature size, and for the mean free path between line of sight encounters with the interstellar features. Additional parameters including the scale height of the O^{+5} feature distribution and the Local Bubble radius are chosen ab initio from other considerations.

As we shall describe in detail in later sections, there are four significant differences between our analysis and that of Jenkins (1978b, c). We allow a local contribution, exclude no stars as anomalous, use a distance-dependent χ^2 test, and slightly revise the probability integral. In general, when the possibility of a local contribution is incorporated into the analysis the quality of the best models rises dramatically over those found without a local contribution. Because all of the low column densities are absorbed into the local contribution, only the larger and more variable ones remain to be explained by hot interstellar regions. As a result, the preferred mean feature column density, $\overline{N_o}$, increases. When the 10 stars identified by Jenkins as anomalous are included in the data set the mean density and the preferred $\overline{N_o}$ are larger. The quality of fits is good. When the distance-dependent χ^2 test is used, the range of acceptable feature and Local Bubble column densities shrinks to a more realistic subset than identified by the old test and the statistical accuracy improves. Finally, our revised version of the probability integral prefers somewhat larger values of $\overline{N_o}$ and in the Monte Carlo simulations is found to be more reliable than Jenkin's version in recovering the true state.

Our reanalysis shows that regions of hot gas (or the interfaces between hot gas and cooler material) are much less frequently encountered in the interstellar medium (ISM) than was indicated by Jenkin's (1978b) work. In addition, a component of $\sim 1.6 \times 10^{13}$ cm^{-2}, possibly due to the Local Bubble, is the only O^{+5} observed for about one-third of the sight lines. Most of the others traverse only one or two additional O^{+5} regions, each of substantial column density. As discussed in § 7.2, this fact is easy to reconcile with pictures in which most of the volume is merely warm, while the O^{+5} is in discrete bubbles of hotter gas. It is more difficult to rationalize with any view in which most of space is filled with hot gas.

When discussing the potential contribution of the Local Bubble, it is important to recognize that there are several possible sites for the ion: in the hot gas in the interior of the bubble, at the outer boundary, at the inner boundary with the Local Cloud (a very local region of warm gas immersed in the bubble; Bertaux et al. 1985; Chassefière et al. 1986), and at boundaries of similar nearby clouds within the Local Bubble. For simplicity, we refer to the net effect as that of the Local Bubble or as the local contribution. Comparison of our results with models of these sites appears in § 7.1.2.

The Local Bubble contribution also stands out in the column density histogram shown in Figure 1. Unlike the statistical method, this figure shows directly those values of column density which are highly probable. There is a single

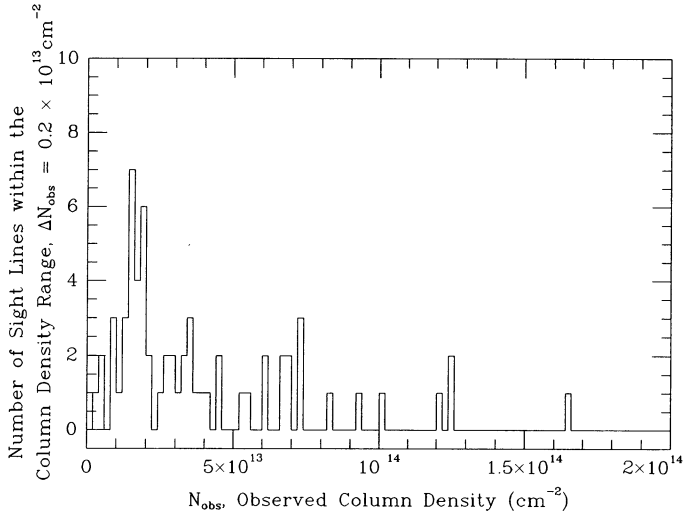

FIG. 1.—Column density histogram; number of lines of sight within various ranges of observed column density. Sight lines without detected column density in the 1032 Å line are excluded. The single strong peak below 2.2×10^{13} cm^{-2} is consistent with the Local Bubble contribution found by the statistical analysis.

strong peak spanning the range 1–2.2×10^{13} cm^{-2}, with a maximum at about 1.6×10^{13} cm^{-2}. It represents nearly one-third of the stars and coincides with the column density range identified by our analysis as belonging to the Local Bubble.

We have examined the distance distribution of stars within this peak (§ 4). They are widely distributed (e.g., Figs. 2 and 3), nearly all beyond 100 pc, and their proportion to the total sample decreases slowly with increasing distance. We regard these characteristics as confirming both our identification of this peak as the Local Bubble contribution[2] and our finding

[2] Though these effects would also be present if an O^{+5} region of significant column density surrounded each star, in § 7.1 we find no evidence supporting a circumstellar hypothesis.

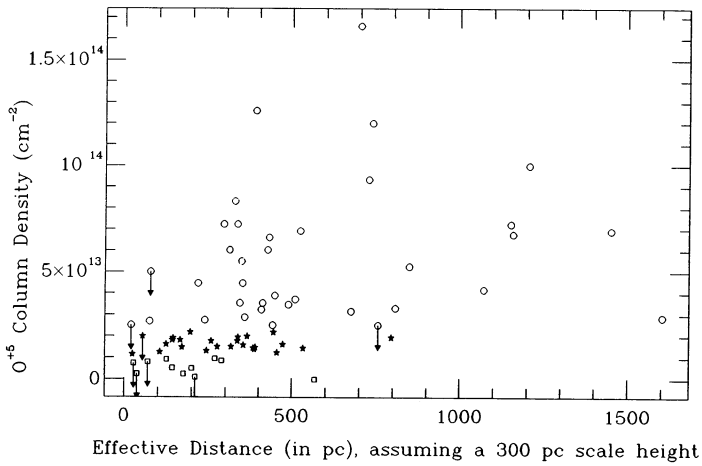

FIG. 2.—O^{+5} column density vs. distance for a 300 pc scale height. Column densities attributed to the Local Bubble are indicated by stars. Most of the smaller column density sight lines (open squares) are within 200 pc of the Sun, and possibly within an anisotropic Local Bubble. Larger column densities (empty circles) are extremely rare to effective distances of 300 pc. Beyond that distance, large column densities are increasingly common but not with increasing magnitude. The statistical analysis infers that large interstellar features exist with several hundred parsec mean free paths between them.

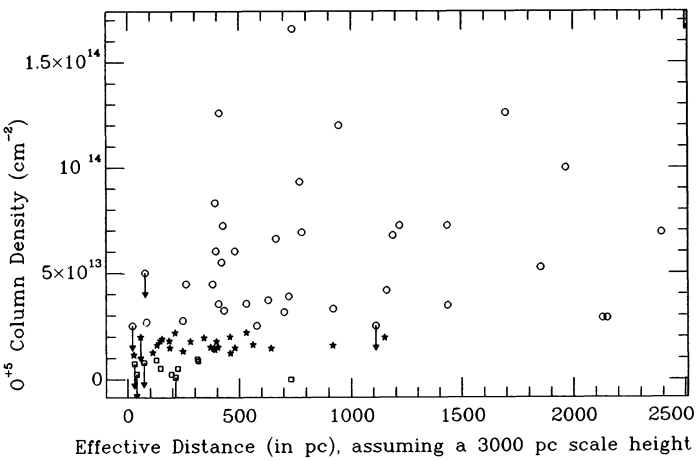

FIG. 3.—Same as Fig. 2 but with a 3000 pc scale height

that there is a long mean free path per encounter with features beyond the Local Bubble.

Having identified this low column density (LCD) subset of the profiles, we present a study of the kinematics of the local hot gas in § 7.1. The data are discussed in § 2. Our method and results are discussed more comprehensively in §§ 3 and 4. In § 5, we apply our analysis to computer-simulated data in order to test the method and explore the influences of data errors. In § 6 we present filling factor and scale height calculations that are similar to those done in Jenkins (1978b), but that incorporate the new $\overline{N_o}$ and $\overline{N_{lb}}$. Our results are compared with modeled $\overline{N_o}$ and $\overline{N_{lb}}$ for candidate structures (i.e., stellar wind bubbles and old SNRs) in § 7. A final summary is presented in § 8.

2. DATA

The O^{+5} ion has two UV resonance transitions, one at 1032 Å and one at 1038 Å, the 1032 Å line being the stronger and more often measured of the two. Jenkins gave preference to this line in his study. The line suffers a near coincidence with the 6–0 $R(0)$ line of HD, but Jenkins (1978a) observed another HD line and subtracted the implied HD contribution from 1032 Å absorption. The 72 *Copernicus* sight lines he selected constitute nearly all of the Galactic observations that are not in directions of conspicuous supernova remnants. We have used nearly the same set in this analysis.[3] The data are presented in Jenkins (1978a) and were used to create the plots of column density versus equivalent distance provided in § 1.

The analysis of these data faces a formidable task. The stellar distances are uncertain to 30% (Jenkins 1978a). The column density measures vary in quality, with typical errors of 30%, estimated by comparing the different measures at 1032 and 1038 Å. Broad weak components and high-velocity components may have gone undetected. The sight lines do not randomly sample the interstellar medium (ISM), both because all end on Earth, and because of limitations on the stars which could be observed. The sight lines all necessarily have low reddening, biasing away from regions in which clouds are common. The stars are all types O and B, which tend to be clustered (nonindependent samples), and may lie within bubbles of hot gas of their own making (biased samples). Finally, soft X-ray observations suggest that the solar location is surrounded by 10^6 K gas in an anisotropic Local Bubble (e.g., Snowden et al. 1990), and that a significant fraction of the sky is subtended by a neighboring bubble, Loop I. Both cause bias in observations made from Earth.

Despite all the complications, a straightforward analysis may provide at least a rough idea of the typical O^{+5} column density, and a fairly good idea of the mean volume density.

3. METHOD

Jenkins assumed that, on average, the O^{+5} volume density falls off exponentially with

$$\bar{n} = \overline{n_o} e^{-|r \sin b|/h}, \quad (1)$$

where $\bar{n}$ and $\overline{n_o}$ are the average O^{+5} volume densities at $|z| = |r \sin b|$ and at the Galactic midplane, respectively. The scale height is h, the stellar distance is r, and the Galactic latitude is b. Generalizing to individual sight lines, the expected O^{+5} column density on a sample line of sight is

$$\int_0^r \bar{n}(r', b, h)dr' = \bar{n}_o h(1 - e^{|-r \sin b|/h}) \csc b . \quad (2)$$

From this relationship he defined the effective distance or equivalent path length in the Galactic plane, r_e, where $r_e = h(1 - e^{|-r \sin b|/h}) \csc b$. The expected total column density along the line of sight is simply $\overline{n_o} r_e(r, b, h)$.

This process eliminates b from further consideration and simplifies the understanding of one of the most important attributes of the data, the relationship between observed column density and effective distance, shown in Figures 2 and 3 for assumed scale heights of 300 and 3000 pc, respectively.

The complications introduced by the local O^{+5} can be easily incorporated into these concepts. The best estimate of the effective distance or equivalent path length beyond the Local Bubble, r_a, is the old equivalent path length reduced by the Local Bubble radius's equivalent length for that direction, yielding

$$r_a = h(e^{-|R_{lb} \sin b|/h} - e^{-|r \sin b|/h}) \csc b , \quad (3)$$

where R_{lb} is the distance from the Sun to the edge of the Local Bubble. Also, the best estimate of the column density due to hot regions beyond the Local Bubble is the total observed column density, N_{obs}, reduced by the average local O^{+5} column density, $\overline{N_{lb}}$, that is, $\hat{N} = N_{obs} - \overline{N_{lb}}$. An estimator of the mean midplane density beyond the Local Bubble is

$$\hat{n_o} = \sum_i \hat{N}_i / \sum_i r_{a,i} , \quad (4)$$

summed over the sight lines.

With these procedures, we have reduced the analysis to that of an equivalent uniform disk, with a known $\hat{n_o}$, and an expected column density beyond the Local Bubble of $\hat{n_o} r_a$. We must still deal with the randomness of encounters with features, the variability of O^{+5} encountered per feature, and the column density of the Local Bubble.

For a mean feature size of $\overline{N_o}$ and mean density of $\hat{n_o}$, the mean free path between encounters is $\lambda = \overline{N_o}/\hat{n_o}$. For a star with an equivalent distance, r_a. the expected number of features is $x = r_a/\lambda = \hat{n_o} r_a / \overline{N_o}$. The probability of finding j features where x are expected is given by the Poisson probability func-

[3] Jenkins used 1032 Å data for 71 of his 72 sight lines and substituted 1038 Å data for the other (Jenkins 1978b). In contrast, we do not substitute the 1038 Å column density of θ Ara, nor do we include the extra, high-velocity component for 15 Mon mentioned in footnote 1 of Jenkins (1978b).

tion

$$P_x(j) = \frac{e^{-x}x^j}{j!}. \quad (5)$$

Because the sight lines in the data set have different equivalent lengths, it is fruitful to develop a method of uniform intercomparison. Jenkins presents a useful scheme based on $P_x(\geq j)$, the probability of encountering j or more regions along a sight line of length r_a, when $x = r_a/\lambda$ are expected.

This probability is the same as that of encountering j regions in an equivalent distance $\leq r_a$, written $P_{\leq x}(j)$:

$$P_x(\geq j) = P_{\leq x}(j) = \sum_{k=j}^{\infty} P_x(k). \quad (6)$$

Similarly, the probability of encountering more than j regions is $P_x(>j)$, which is equal to $P_x(\geq [j+1])$ because j is limited to integer values. Then, because

$$\frac{d}{dr}[P_x(j)] = \frac{P_x(j-1) - P_x(j)}{\lambda},$$

where r is the distance variable, we have

$$\frac{d}{dr}[P_x(\geq j)] = \frac{P_x(j-1)}{\lambda}$$

and

$$\frac{d}{dr}[P_x(>j)] = \frac{P_x(j)}{\lambda}.$$

Therefore, with $dx = dr/\lambda$,

$$P_x(\geq j) = \int_0^{r_a\hat{n}_o/\overline{N_o}} P_x(j-1)dx. \quad (7)$$

Similarly,

$$P_x(>j) = \int_0^{r_a\hat{n}_o/\overline{N_o}} P_x(j)dx. \quad (8)$$

Following Jenkins (plus supporting theoretical experiments), we accommodate the dispersion of individual feature column densities by generalizing the discrete distributions of equations (7) and (8) into a continuous distribution in column density, obtaining a good approximation to the probability of finding a total column density beyond the Local Bubble which is greater than N. In the continuous distribution, the distinction between probability $\geq N$ and merely N must disappear. Therefore, the best approximation to the continuous P lies intermediate between equations (7) and (8). For $j > 0$, replacing the discrete j with the continuous v $(= N/\overline{N_o})$ yields

$$P_x(\geq v) \cong \int_0^{r_a\hat{n}_o/\overline{N_o}} P_x\left(v - \frac{1}{2}\right)dx = \frac{1}{\Gamma(v+1/2)}\int_0^{r_a\hat{n}_o/\overline{N_o}} e^x x^{v-1/2}\,dx, \quad (9)$$

where $P_x(\geq v) = P_x(>v)$.

This form differs somewhat from that in Jenkins (1978b), which used v instead of $v - \frac{1}{2}$ in the above integral, ignoring the small shift required in converting to the continuous distribution. Another way to understand the need for this alteration is that $P_x(v)$ is the average derivative with respect to v of our integral between $v - \frac{1}{2}$ and $v + \frac{1}{2}$, while it is the average derivative of Jenkin's integral between $v - 1$ and v. The difference between the two is small when v is large, that is when the column density to a star arises from many small contributions.

The variation in the Local Bubble column density can be taken into account by making two simple modifications. The best estimate of the column density beyond the Local Bubble, $\hat{N}$, must be used where the exact value, N, was used in equation (9) and in the definition of v. Second, the contribution from $j = 0$ in equation (5) must be broadened and included explicitly. In principle, the distribution in equation (9) should be broadened slightly, in order to characterize the added variation in $N_{\rm obs}$ due to the variation in Local Bubble column density, but this effect is largely unnoticeable.

The second step is accomplished by approximating the differential probability of observing a given column density, $\mathcal{N}$, as an inverted parabola with zeros at 0 and $2\overline{N_{\rm lb}}$ and area equal to $P_x(0)$.[4] The functional form used is: $[3P_x(0)/4\overline{N_{\rm lb}}]\{1 - [(\mathcal{N} - \overline{N_{\rm lb}})/\overline{N_{\rm lb}}]^2\}$. Then, for $j = 0$ and $\mathcal{N} \leq 2\overline{N_{\rm lb}}$ the probability that the observed column density should have been $\geq N_{\rm obs}$ is $P_x(0)$ minus the integral of the differential probability from $\mathcal{N} = 0$ to $N_{\rm obs}$. This is

$$P_x(0)\left\{1 - \frac{1}{4}\left[2 + 3\left(\frac{N_{\rm obs} - \overline{N_{\rm lb}}}{\overline{N_{\rm lb}}}\right) - \left(\frac{N_{\rm obs} - \overline{N_{\rm lb}}}{\overline{N_{\rm lb}}}\right)^3\right]\right\}. \quad (10)$$

The Local Bubble modification can be completed by combining the $j = 0$ contribution with that of $j > 0$. For $N_{\rm obs} < 2\overline{N_{\rm lb}}$, the $j = 0$ contribution is given by equation (10), otherwise it is 0. Although equation (9) does not explicitly include the slight broadening due to variations in the Local Bubble column density, it is already smooth and can be used as the $j > 0$ contribution. It must, however, be limited to $\leq [1 - P_x(0)]$ which is the summed probability for $j \geq 1$. Thus, our approximation of the total probability, $\mathcal{P}_x(\geq v)$ or $\mathcal{P}_{\leq x}(v)$, is

$$\mathcal{P}_x(\geq v) = \left\{\begin{array}{l} P_x(0)\left\{1 - \frac{1}{4}\left[2 + 3\left(\frac{N_{\rm obs} - \overline{N_{\rm lb}}}{\overline{N_{\rm lb}}}\right) - \left(\frac{N_{\rm obs} - \overline{N_{\rm lb}}}{\overline{N_{\rm lb}}}\right)^3\right]\right\} \\ \qquad\qquad \text{if } N_{\rm obs} \leq 2\overline{N_{\rm lb}} \\ 0 \quad \text{if } N_{\rm obs} > 2\overline{N_{\rm lb}} \end{array}\right\} + \left\{\begin{array}{l} \text{minimum of} \\ \frac{1}{\Gamma(v+1/2)}\int_0^{r_a\hat{n}_o/\overline{N_o}} e^x x^{v-1/2}\,dx \quad \text{or} \quad [1 - P_x(0)] \end{array}\right\} \quad (11)$$

where $v = (N_{\rm obs} - \overline{N_{\rm lb}})/\overline{N_o}$. This function is our final approximation to the probability of encountering a total column density exceeding that observed.

For each assumed set of $\overline{N_{\rm lb}}$, h, and $R_{\rm lb}$, the estimated mean density, $\hat{n}_o$ is calculated from equation (4). Then, assuming an $\overline{N_o}$, the probability, $\mathcal{P}_x(\geq v)$, is evaluated for each of the stars beyond the Local Bubble. When $\overline{N_{\rm lb}}$ is taken to be nonzero, all values of $\mathcal{P}_x(\geq v)$ between 0 and 1 should be equally likely and a χ^2 test can be used to determine the goodness of fit between the data set and the Poisson model at a given $\overline{N_o}$ and $\overline{N_{\rm lb}}$. Excluding sight lines which may be inside of the Local Bubble, our data set includes two sight lines with only upper limits to

[4] For comparison, we also examine the data with other forms of a Local Bubble distribution, including more concentrated functions, a flat function, and a delta function. In each of these cases, the resulting best fit values of $\overline{N_o}$ and $\overline{N_{\rm lb}}$ are relatively constant, though the likelihood of worse fit is much lower when a delta function is used and the more likely values of $\overline{N_o}$ are slightly smaller when a very concentrated distribution is assumed.

their column densities. Like Jenkins, we assume that the true column densities could be any value between 0 and the upper limit, so these sight lines are apportioned between all of the probability intervals equal to and above the interval that $\mathscr{P}_x(\geq v)$ would correspond to if a column density had been detected at the upper limit.

When $\overline{N_{lb}}$ is assumed to be 0, however, $\mathscr{P}_x(\geq v)$ makes a sudden transition from 1 at $N_{obs} = 0$ to $1 - P_x(0)$ for very small N_{obs}. Thus, all values of $\mathscr{P}_x$ are not equally likely for sight lines with detected column densities. To return the overall distribution to uniform, sight lines with no intercepted O^{+5} must have their probabilities reapportioned evenly between $1 - P_x(0)$ and 1. For such a sight line, the observation should have provided only an upper limit to its column density, and therefore both we and Jenkins correctly reapportion its contribution to the probability histogram.

It is more generous to the $\overline{N_{lb}} = 0$ hypothesis to take this procedure a step further. Perhaps, due to experimental uncertainty or other causes, a few of the lines of sight with very low recorded column densities actually do not traverse the O^{+5} regions that we are modeling. Therefore, their probabilities should be reapportioned evenly between $1 - P_x(0)$ and 1, and their observed column densities should be treated as zeros. We tried this approach, considering various column density cutoffs including 0.5, 0.6, and 1.0×10^{13} cm^{-2}. The cutoff value should be less than about half of the $\overline{N_o}$ being considered so that sight lines that encounter a single interstellar feature are not mistakenly assumed to have encountered no such features. The cutoff should also be realistic, considering the size of the experimental uncertainty. For the results presented below, 0.6×10^{13} cm^{-2} was adopted as a reasonable value.

When the χ^2 test is performed using 10 equally spaced probability intervals, high likelihoods of worse fit can be found over considerable ranges of $\overline{N_o}$ and $\overline{N_{lb}}$. But, some combinations of $\overline{N_o}$ and $\overline{N_{lb}}$ favored by this test show significant and unacceptable trends of $\mathscr{P}_x(\geq v)$ with r. In one common trend, nearby stars tend to have small $\mathscr{P}_x(\geq v)$, while far stars have higher values. For example, this phenomenon occurs for a small value of $\overline{N_{lb}}$ and $\overline{N_o}$ chosen from the $h = 300$ pc case of Figure 4. The integrated probabilities are shown versus equivalent distance beyond the Local Bubble in Figure 5. Trials on simulated data suggest that this trend results from an underestimation of the Local Bubble contribution. Another type of trend is concentration of probability to the midrange at large distances (see Fig. 6) and is symptomatic of assuming an overly large value for $\overline{N_o}$. The quality of fit statistic cannot detect these trends and thus has too broad a window of acceptability in the parameters. In contrast, using a simple distance-dependent test significantly reduces the range of acceptable parameters and finds solutions that acceptably represent both long and short sight lines. In addition, the new test assigns a more reasonable quality of fit to the true $\overline{N_o}$ and $\overline{N_{lb}}$ in Monte Carlo simulations.

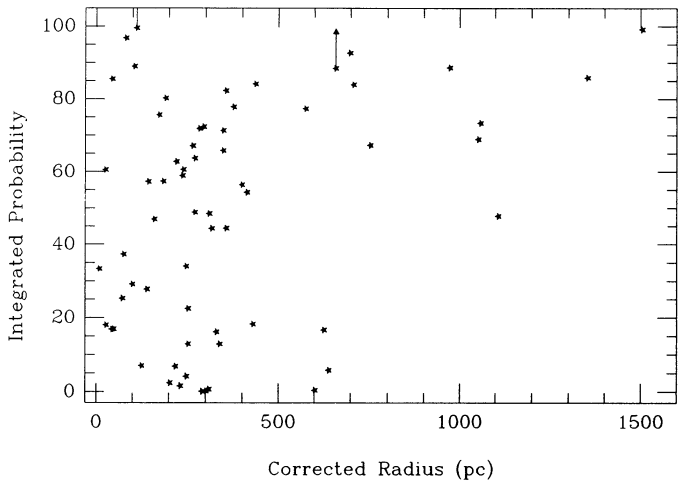

FIG. 5.—Plot of integrated probability vs. equivalent distance beyond a 100 pc Local Bubble for $\overline{N_{lb}} = 1.0 \times 10^{13}$ cm^{-2} and $\overline{N_o} = 2.2 \times 10^{13}$ cm^{-2}. The upward arrows signify lower limits on the integrated probability, which are due to upper limits on the column density. Using the regular χ^2 test, the likelihood of worse fit for this case is 44%.

Our method, hereafter referred to as the distance-sensitive χ^2 test, guards against these unwarranted trends by testing that probabilities are uniformly distributed between 0 and 1, independent of distance. Specifically, we separate the data set into near ($r_a \leq 400$ pc) and far stars ($r_a > 400$ pc), with five equal probability bins for each. With this binning, the uniformity over $\mathscr{P}_x(\geq v)$ and distance independence of that uniformity are evaluated simultaneously. Because there are 10 bins and four parameters, six degrees of freedom are used when calculating the likelihood of worse fit from the value of χ^2. In tests with simulated data, the more compact range of $\overline{N_o}$ and $\overline{N_{lb}}$, found

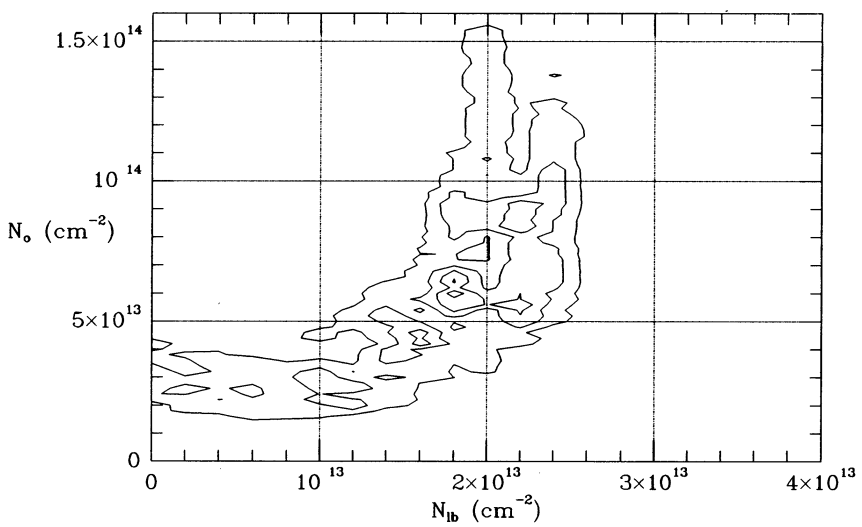

FIG. 4.—10%, 30%, 50%, and 70% contours of likelihood of worse fit vs. $\overline{N_o}$ and $\overline{N_{lb}}$ found with the regular χ^2 test for $R_{lb} = 100$ pc and $h = 300$ pc

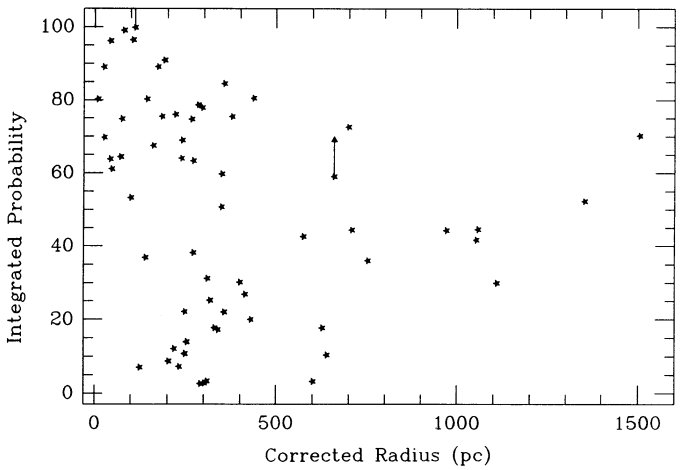

FIG. 6.—Plot of integrated probability vs. equivalent distance beyond the Local Bubble for $\overline{N_{\rm lb}} = 2.2 \times 10^{13}$ cm^{-2}, $\overline{N_o} = 8.4 \times 10^{13}$ cm^{-2}, $R_{\rm lb} = 100$ pc, $h = 300$ pc. The likelihood of worse fit found from the regular χ^2 test is 68%. The trends of probability with distance in Figs. 5 and 6 motivates the use of a distance-sensitive test.

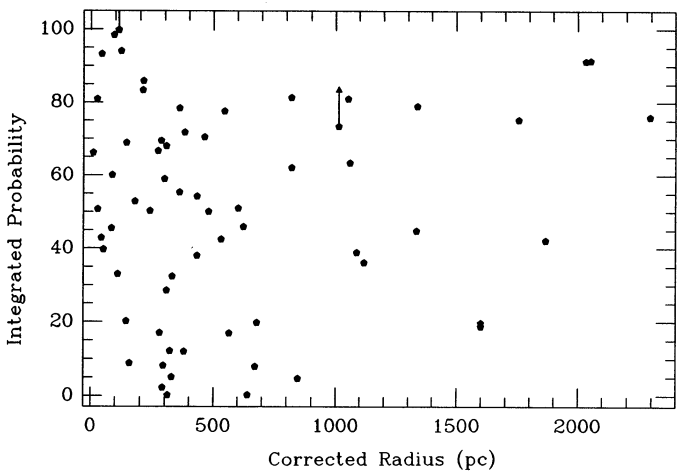

FIG. 8.—Plot of integrated probability vs. effective distance beyond the Local Bubble: the integrated probabilities were obtained with eqn. (11), with $\overline{N_o} = 3.6 \times 10^{13}$ cm^{-2}, $\overline{N_{\rm lb}} = 1.6 \times 10^{13}$ cm^{-2}, a 3000 pc scale height, and a 100 pc Local Bubble radius. The likelihood of worse fit for this case is 80%. With a large scale height and the distance-sensitive χ^2 test, the analysis finds model parameters that reproduce the expected distribution of probability.

with the distance-dependent test, generally overlaps part of the larger range preferred by the regular test in the region of the input parameters of the simulation.

Integrated probabilities for likely values of $\overline{N_o}$ and $\overline{N_{\rm lb}}$, found with the distance-sensitive χ^2 test, are plotted against equivalent distances beyond the Local Bubble in Figure 7. Figure 8 presents the same information when a 3000 pc scale height is assumed. Because our method has coarser binning in $\mathscr{P}_x(\geq v)$, it is less sensitive to peculiarities that strike first at the upper and lower limits of $\mathscr{P}_x(\geq v)$. It would be best to use both binning methods and accept only results admissible by both.

Clearly, the new plots are free of the distance dependent probability trend exhibited in Figure 5. Nevertheless, the new plot for $h = 300$ pc shows several long equivalent length sight lines clustered toward medium probabilities. This implies that these six sight lines could be better modeled with a smaller $\overline{N_o}$ than was chosen, while remaining sight lines would be less well modeled. This phenomenon can simply result from small number statistics (six stars), or from distant, small wisps of O^{+5} being intermixed with the larger features. It cannot result directly from a halo phenomenon because none of these six stars is at a height over 400 pc. Much of this trend disappears for the $h = 3000$ pc case, for which the analysis chooses a somewhat lower value of $\overline{N_o}$.

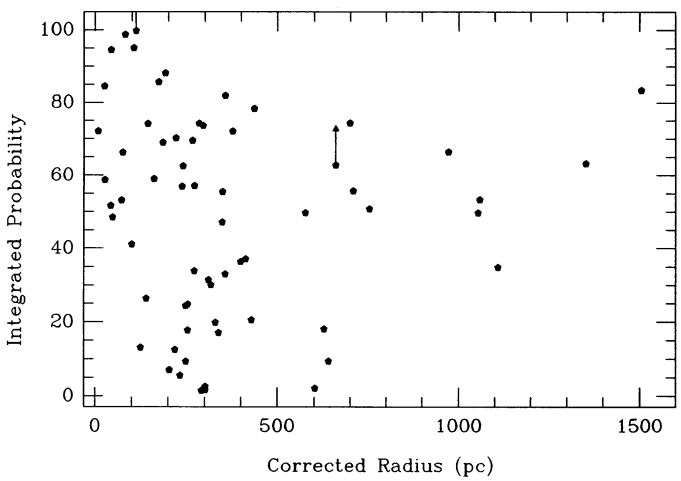

FIG. 7.—Plot of integrated probability vs. effective distance beyond the Local Bubble: eq. (11) was used, with $\overline{N_o} = 5.4 \times 10^{13}$ cm^{-2}, $\overline{N_{\rm lb}} = 1.8 \times 10^{13}$ cm^{-2}, a 300 pc scale height, and a 100 pc Local Bubble radius giving a likelihood of worse fit of 84%. Introduction of the distance-sensitive χ^2 test has forced the analysis to find model parameters that represent both nearby and more distant stars. Implications of the remaining trend are discussed in the text.

4. RESULTS

We determined the most likely values of $\overline{N_o}$ and $\overline{N_{\rm lb}}$ by calculating the likelihood of worse fit between the model and data for different combinations of $\overline{N_o}$ and $\overline{N_{\rm lb}}$. Values of $\overline{N_o}$ between 0.2×10^{13} and 16.0×10^{13} cm^{-2} were tested with a trial every 0.2×10^{13} cm^{-2}, while $\overline{N_{\rm lb}}$ ranged from 0 to 4.0×10^{13} cm^{-2}, also sampled every 0.2×10^{13} cm^{-2}. Because the O VI scale height may be as low as 300 pc or as great as that of the other high-stage ions, we tried both 300 and 3000 pc. Also, the Local Bubble radius is not well determined, so we repeated the above using three different assumed radii: 50, 100, and 150 pc, spanning the probable range.

Examples of the resulting likelihood of worse fit versus $\overline{N_o}$ and $\overline{N_{\rm lb}}$ are presented in contour form assuming a 100 pc Local Bubble radius and a 300 or 3000 pc scale height in Figures 9 and 10, respectively. With a 300 pc scale height and 100 pc Local Bubble radius (Fig. 9), the likelihood of worse fit peaks at 86% and is 50% or greater only for $\overline{N_o}$ between 4.2 and 6.6×10^{13} cm^{-2} (not corrected for the 0.6×10^{13} cm^{-2} bias discussed in § 5) and $\overline{N_{\rm lb}}$ between 1.6 and 1.8×10^{13} cm^{-2}. Since some of the observed column density is in the Local Bubble, the O^{+5} midplane volume density beyond the Local Bubble is somewhat less than the total sight line average of 2.8×10^{-8} cm^{-3}, the range being 2.0–2.1 $\times 10^{-8}$ cm^{-3}. The corresponding mean free path between sight line encounters with hot gas regions is between 650 and 1100 pc.

For the 3000 pc scale height and 100 pc Local Bubble radius (Fig. 10), the likelihood of worse fit peaks at 81% and is 50% or greater only for $\overline{N_o}$ between 2.0 and 5.0×10^{13} cm^{-2} (also uncorrected for bias) and $\overline{N_{\rm lb}}$ between 1.4 and 1.8×10^{13}

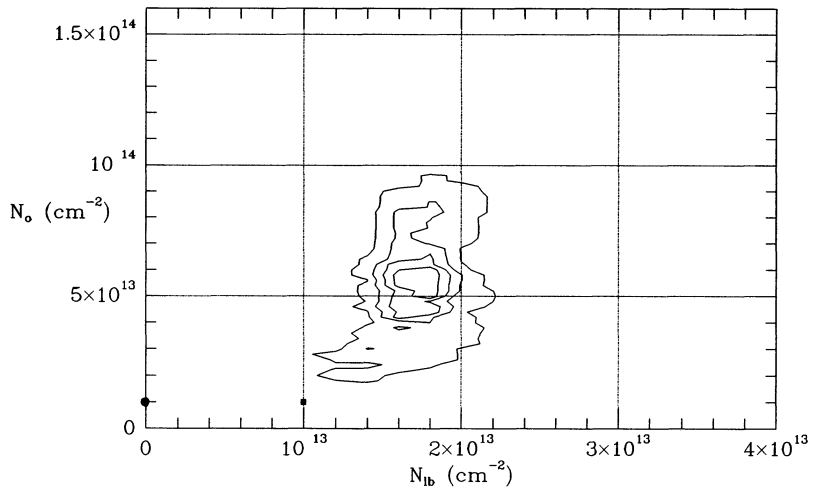

FIG. 9.—10%, 30%, 50%, and 70% contours of likelihood of worse fit vs. $\overline{N_o}$ and $\overline{N_{lb}}$ for $R_{lb} = 100$ pc and $h = 300$ pc. The filled circle and square indicate values preferred, respectively, by Jenkins (1978b) and (1978c). The 1978b work assumed $R_{lb} = 0$ and $N_{lb} = 0$. The 1978c work used $R_{lb} = 100$ pc.

cm^{-2}. The O^{+5} midplane volume density beyond the Local Bubble is 1.3–1.5 × 10^{-8} cm^{-3}; the mean free path is between 450 and 1300 pc.

Using the other values for the Local Bubble radius only slightly increases the range of likely $\overline{N_o}$, $\overline{N_{lb}}$, n_o, and λ. The extremes of the 50% contour level for all cases are presented in Table 1. The results can be compared with those found with the distance-independent χ^2 test. As shown in Figure 4 (for $h = 300$ pc and $R_{lb} = 100$ pc), the distance-independent test gives high likelihoods of worse fit to a few distinct patches of $\overline{N_o}$ and $\overline{N_{lb}}$, some of which overlap with the high likelihood regions found with the distance-dependent test. For this scale height and Local Bubble radius, requiring that both tests give at least 50% likelihood of worse fit returns the same values given in Table 1. For the larger scale height and $R_{lb} = 100$ pc, requiring success with both tests further constrains the average feature column density to 2.8–5.0 × 10^{13} cm^{-2} and the average mean free path to 600–1300 pc.

Assuming a 300 pc scale height and no Local Bubble, Jenkins found the midplane volume density, $\bar{n}_o$, to be 2.8 × 10^{-8} cm^{-3}, or 2.1 × 10^{-8} cm^{-3} if "anomalous"[5] sight lines are excluded. These are similar to ours, but his mean free path and $\overline{N_o}$ are about 4–7 times smaller (165 pc and 1.05 × 10^{13} cm^{-2}, respectively) than ours for $h = 300$ pc and $R_{lb} = 100$ pc. Having carefully explored the factors leading to this difference, we are confident that our results are appropriate unless the Local Bubble does not contribute significantly to the observed O^{+5}.

Inspection of the column density versus distance data further enhances our confidence in these models:

1. Of the seven stars closer than 80 pc, only one has detected interstellar O^{+5} and three have column densities less than 0.8 × 10^{13} cm^{-2}.
2. Although the bubble boundary may be as much as 200 pc away in some directions, most of the stars in our sample

[5] The 10 sight lines with the highest detected volume densities poorly fit Jenkins's model, while the remaining sight lines appeared to fit well. The 10 sight lines were subsequently labeled "anomalous" and are identified in Jenkins (1978a).

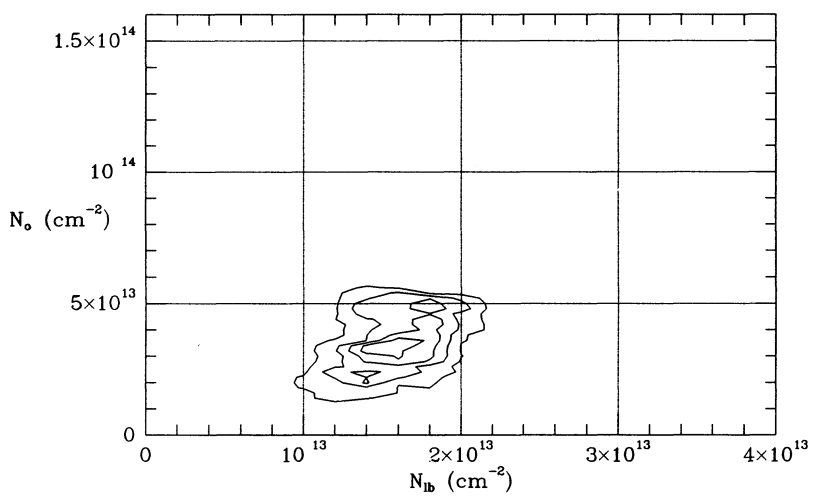

FIG. 10.—10%, 30%, 50%, and 70% contours of likelihood of worse fit vs. $\overline{N_o}$ and $\overline{N_{lb}}$ for $R_{lb} = 100$ pc and $h = 3000$ pc. In both Figs. 7 and 8, the analysis prefers only Local Bubble column densities consistent with the histogram peak in Fig. 1, and a column density per interstellar feature considerably greater than Jenkin's value.

TABLE 1

LIKELY VALUES OF $\overline{N_o}$, $\overline{N_{lb}}$, $\widehat{n_o}$, AND λ

Scale height (pc)	R_{lb} (pc)	$\overline{N_o}$ (10^{13} cm^{-2})	$\overline{N_{lb}}$ (10^{13} cm^{-2})	$\widehat{n_o}$ (10^{-8} cm^{-3})	λ (pc)
3000.....	150	3.4–5.4	1.6–2.0	1.3–1.5	700–1350
	100	2.0–5.0	1.4–1.8	1.3–1.5	450–1300
	50	2.6–4.8	1.2–1.8	1.2–1.5	550–1350
300.....	150	4.2–6.8	1.8	2.3	600–950
	100	4.2–6.6	1.6–1.8	2.0–2.1	650–1100
	50	2.8–7.0	1.2–1.8	1.8–2.2	400–1300

NOTES.—The likelihood of worse fit for a random sample of a population governed by the model reached 50% only within these ranges in $\overline{N_o}$, $\overline{N_{lb}}$, $\widehat{n_o}$, and λ, given the specified h and R_{lb}. We have not reduced these values of $\overline{N_o}$ by 0.6×10^{13} cm^{-2} to counteract the analysis's tendency to overestimate that parameter. Nor have we broadened the ranges in response to the analysis's proclivity to underestimate the goodness of fit.

between 100 and 300 pc should lie outside the Local Bubble. Of the 18 target stars in this interval, only two have column densities below 10^{13} cm^{-2} (π Sco and γ Cas), while only three have interstellar column densities above 2.2×10^{13} (α Vir, μ Sco, and λ Eri). The remaining 13 all have values in the range we attribute to the local component.

3. Eight more target stars are between 300 and 400 pc: six with $1.0–2.2 \times 10^{13}$ cm^{-2}, none with a lower value, and two with much higher values (4.5×10^{13} cm^{-2} for γ^2 Vel in the Gum Nebula and 8.3×10^{13} cm^{-2} for HD 36695 in Orion). Thus, all of these stars appear to be beyond the Local Bubble boundary, while the latter two are beyond an additional O^{+5}-rich region.

4. Though 10 sight lines are identified as "anomalous" in the analysis by Jenkins, their column densities are easily within the expected range when a Local Bubble and large common features are assumed. For example, Jenkin's choice of $\overline{N_o}$ and no Local Bubble requires very low column densities for nearby stars, but short dense sight lines are acceptable when the Local Bubble and Local Cloud interface provide that O^{+5}. Medium length, column-dense sight lines are also unacceptable in his model, while in ours these require only one additional feature beyond the Local Bubble. Likewise, longer lines of sight can comfortably provide quite large column densities either by encountering a modest number of additional features or by encountering a single feature with unusually large strength.

5. A component of $1–2 \times 10^{13}$ cm^{-2} is normally acquired at distances between 80 and 200 pc, distances which are very similar to the range estimated for the boundary of the Local Bubble. Furthermore, our estimate of the large mean free path to additional hot gas features is supported by the fact (evident in Figs. 2 and 3) that nothing other than the Local Bubble has been encountered for most effective sight lengths less than 300 pc. Based on this inspection, it appears that the statistical approach has succeeded.

The original modeling (Jenkins 1978b) examined the case without a Local Bubble. Using our analysis we have also evaluated models with $R_{lb} = 0$ and $\overline{N_{lb}} = 0$.[6] We analyze this case with two data sets: the full set and a set without the "anomalous" sight lines. Clearly, varying the exclusiveness of the data set influences the goodness of fit and the preferred $\overline{N_o}$, therefore implying an increased number of free parameters in the χ^2 test, while the loss of variation in the Local Bubble column density implies a loss of a free parameter. To accommodate all tastes in this matter, we provide probability of worse-fit results for both 6 and 7 degrees of freedom.

As would be expected, the better models without a Local Bubble have much smaller mean feature column densities because they must reproduce the low column densities (which we attribute to the Local Bubble) seen toward many relatively nearby stars. For models including the entire data set, using our analysis and assuming a 300 (or 3000) pc scale height, the most likely $\overline{N_o}$ is 2.6 (or 2.0) $\times 10^{13}$ cm^{-2}. The unreduced χ^2 values are quite large, however, giving 16 (or 23)% likelihoods of worse fit using 6 degrees of freedom and 23 (or 32)% using 7 degrees of freedom (d.o.f.). The models cannot comfortably accommodate the observed mixture of high and low average line-of-sight volume densities.

The fit quality can be improved remarkably by excluding Jenkins's 10 "anomalous" lines of sight from the data set. For either scale height, the preferred $\overline{N_o}$ is 1.2×10^{13} cm^{-2}, with 82 (or 48)% likelihoods of worse fit using 6 d.o.f. and 89 (or 60)% using 7 d.o.f. for 300 (or 3000) pc scale height, respectively. Discarding the stars with the largest mean line of sight densities (the "anomalous" data) narrows the scatter in N/r_a, indicating a smaller λ and $\overline{N_o}$. In addition, this culling of the data lowers $\overline{n_o}$, reducing $\overline{N_o}$ even further.

5. SIMULATIONS

The ability of our analysis technique to extract meaningful parameter estimates was tested by applying it to simulated data sets, extracted from our basic model and enriched with measurement errors.

In such explorations, it is important to use the observed distribution of stars over distance and the same sample size for the test; consequently, we adopted the actual number of stars and the published distances for each data set. The only variable quantity was the column density, N_{obs}, for each star.

In order to assess the importance of measurement errors in both stellar distance and column density, we assumed that the published distances were in error by a random amount with standard deviation of 20%.[7] For each data set, each star was assigned a true distance found by subtracting a random error. This true distance was then modified to an effective distance (depending on the assumed O VI scale height), an integrated probability function for column density was evaluated (depending on model values for $\overline{N_o}$, $\overline{N_{lb}}$, and $\widehat{n_o}$, and dispersions in the first two), and a random value for the column density, N, was chosen, consistent with that probability. A random error was then added, also with 20% standard deviation, to obtain N_{obs}, the simulated observed column density for the star. The assumed true distance was then discarded, leaving the data pair r_{obs}, N_{obs}. This process was repeated for each star to complete a simulation set.

The simulation sets thus have independent choices of column density for each star, despite the fact that the real sight lines are somewhat clustered and therefore are not independent samples. We tested the significance of ignoring such clustering by including multiple copies of stars in an analysis of the actual

[6] Note that the following results do not coincide with Figures 9 and 10 because this analysis requires $R_{lb} = 0$, while those figures require $R_{lb} = 100$ pc. As previously discussed, for models with $\overline{N_{lb}} = 0$ only, column densities below 0.6×10^{13} cm^{-2} were assumed to be due to observational uncertainty or spurious effects and were reset to zero. This technique reduces the χ^2.

[7] Both larger and smaller random errors were tried, with similar results.

data, with the result that having a star included four times does not change our outcomes significantly.[8]

Many simulated sets were constructed and analyzed for the same input parameters, to assess random variability of the outcome of the analysis at fixed parameters. In addition, a variety of model parameters were examined to explore their influence on the mean outcome.

Our first concern was to check that the analysis results actually track the input parameters, rather than, for example, giving the same results for all sets of input parameters, $\overline{N_o}$ and $\overline{N_{lb}}$. We compared the analysis results for a spectrum of input parameters, finding that the analysis does *not* favor certain values and that it generally assigns the higher likelihoods near the input values.

Our second concern was to check that the analysis results are not significantly biased. By analyzing data sets with input parameters and errors similar to those of the real data, for both $h = 300$ and 3000 pc, we found that there is no bias in $\overline{N_{lb}}$ to within 0.1×10^{13} cm^{-2}, but that the analysis does tend to prefer values of $\overline{N_o}$ which are about 0.6×10^{13} cm^{-2} larger than the input value (compared to $\overline{N_o}$ on the order of $2\text{–}7 \times 10^{13}$ cm^{-2}). This bias, however, is not very significant given the size of the likelihood contours.

Our third concern was to check that the likelihood contours are good confidence indicators. Theoretically, if a large number of simulated data sets are made and then evaluated for χ^2 at their input parameters, then half of the sets should have likelihoods between 50% and 100%, three-fourths will have values between 25% and 100%, and so on, (assuming no bias in $\overline{N_o}$ or $\overline{N_{lb}}$). We checked this by performing the statistical analysis on 100 simulated data sets for each of several different parameter sets. We then tallied the likelihoods assigned to the input $\overline{N_{lb}}$ and the input value of $\overline{N_o}$ added to the 0.6×10^{13} cm^{-2} bias. The likelihoods were similar to, but slightly below, the theoretically predicted values. For example, the median likelihood of worse fit evaluated at the input parameters was 40% $\pm$ 5% while it should have been 50%, meaning that our analytical method slightly underestimates the quality of fit.

In addition to these three major inquiries, we used simulated data sets as a testing ground for our version of the integrated probability function and the distance-dependent χ^2 test. After a Local Bubble modification had been added to Jenkins's integral in order to make it comparable with our own, both integrals were used to evaluate simulated data made with $\overline{N_o}$ and $\overline{N_{lb}}$. The new probability function, used with the distance-sensitive χ^2 test, more consistently returned the input parameters and gave more realistic estimates of the goodness of fit than did Jenkins's integral used with either test, or our integral used with the distance-insensitive χ^2 test.

6. SCALE HEIGHT, RADIAL GRADIENT, AND FILLING FACTOR

It is necessary for us to confirm that the assumed scale heights are reasonable when a local column density on the order of 1.6×10^{-13} cm^{-2} is subtracted from the data. In addition, another high-stage ion, C^{+3}, has recently been analyzed for a Galactic radial dependence by Savage et al. (1993) and O^{+5} deserves similar scrutiny.

[8] We repeated the test for six different sight lines, varying in distance and mean line of sight density. The resulting variations in preferred $\overline{N_o}$ and $\overline{N_{lb}}$ are less than between simulation sets drawn from the same model parameters.

Using the same graphical method as Jenkins, but adjusting for a local O^{+5} column density and radius of $N_{lb} = 1.6 \times 10^{13}$ cm^{-2} and $r_{lb} = 100$ pc, respectively, and omitting nearby ($r < 300$ pc) stars, we obtain a log ($\Delta N \,|\sin b|$) versus log $|z|$ plot which exhibits the same trends as Figure 6 in Jenkins (1978b) (see Fig. 11). Other Local Bubble parameters were also tried with similar results. The data set includes six high z sight lines, four of which indicate a z dependence consistent with $h \cong 300$ pc, and two which do not. Thus, the average line-of-sight density is lower for the high z sight lines than for the others. Jenkins's choice for the O VI scale height from this method was 300 pc. Although we might have interpreted his results and ours to imply a slightly higher value, his 300 pc value is a representative lower bound.

Other evidence, however, suggests that a scale height of several kiloparsecs is more likely appropriate. This greater thickness has been found for other high-stage ions (C^{+3}, N^{+4}) whose vertical distributions have been studied much more thoroughly (Savage & Massa 1987; Savage et al. 1993). There is also one extragalactic sight line for which the O^{+5} column density has been measured, toward 3C 273 by *HUT* (Davidsen 1993). The somewhat uncertain but definitely very large column density also implies a large scale height. One might suppose that this is evidence enough to abandon models with low scale heights, but the issue is not so clearly settled. The 3C 273 sight line may be unusual since it passes very near the edge of Loop I. Also, there could well be two or more major contributors to the high-ion data, for example, supernova remnant bubbles with a scale height of order 300 pc (e.g., Slavin & Cox 1992, 1993), microflares with a scale height of order 2 kpc (e.g., Raymond 1992), and a chromospheric outer boundary to the Galactic disk beyond that (e.g., Sciama 1972). If the chromo-

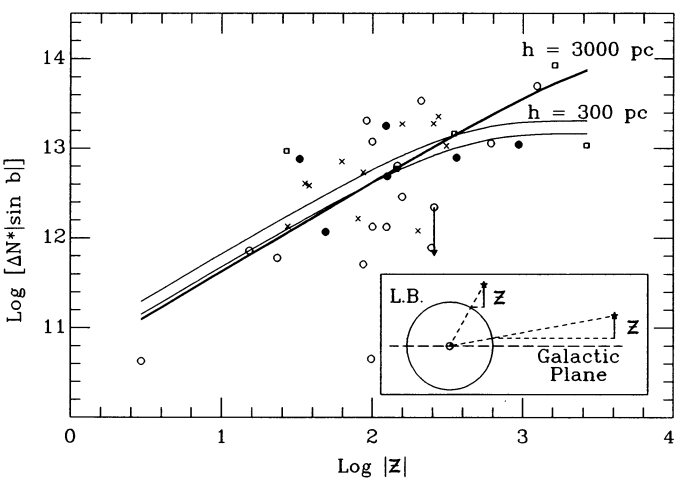

FIG. 11.—Log ($\Delta N \,|\sin b|$) vs. log $|z|$, marked by direction, (filled circles represent lines of sight toward the Galactic center between $l = 315°$ and 45°, while open squares denote $l = 45°\text{–}90°$ and $270°\text{–}315°$, crosses denote $l = 90°\text{–}135°$ and $225°\text{–}270°$, and open circles represent anticenter sight lines, $l = 135°\text{–}225°$) where ΔN and z are the column density beyond and height above the Local Bubble boundary, assuming a Local Bubble column density of 1.6×10^{13} cm^{-2} and a Local Bubble radius of 100 pc. Note from the schematic that at different latitudes, the same z samples a different range of heights and thus a different expected mean column density. The double lines on the graph delimit the expected range, found using $|b| \simeq 0$ to 90° and $h = 300$ or 3000 pc. Sight lines with $r < 300$ pc were excluded. Six additional sight lines with observed column density less than $\overline{N_{lb}}$ were not plotted; one is toward the Galactic center while three point away from it. From this information alone, the full range of scale heights explored is plausible. See discussion in text regarding the radial gradient.

spheric layer is very high and makes a large contribution, extragalactic sight lines will be useless in helping to establish the ion distribution close to the plane. Given this unsettled state of affairs we have explored models with scale heights of 300 and 3000 pc, more or less spanning the possible range.

Considering that the supernova and star formation rates drop rapidly with galactocentric radius, it is highly likely that the O^{+5} population will have a strong radial gradient. Yet, such an effect could be difficult to observe from our location because we are on the *inner* edge of the Orion Arm. Exploring this issue, we found that low-latitude sight lines within 45° of the Galactic center have about 80% more O^{+5} per parsec than do the sight lines within 45° of the anticenter, when the Local Bubble is subtracted and short sight lines are excluded. This may be due to a decrease in O^{+5} with distance from the Galactic center, though large scatter in other directions undermines the significance of the result.

Figure 11 can also be examined for signs of a possible Galactic radial gradient in the O^{+5} distribution. The ratio of anticenter to center sight lines is about the same below the theoretical curves as above. Interestingly, the anticenter sight lines exhibit much more downward scatter, including most of the very low $\Delta N\,|\sin b\,|$ data, while the galactic center data are closer to the calculated averages. This trend, though, is not supported in plots of column density versus equivalent sight length. Consequently, although we see hints of a possible radial dependency, a significant effect has not been established.

It would be extremely useful to know the pervasiveness (filling factor) of O^{+5} bearing hot gas in the ISM, but the available data do not provide unambiguous estimates. For example, if one assumes that the hot gas has a single temperature and is in collisional equilibrium with a pressure $p/k = 10^4$ K cm^{-3}, then the mean density of O^{+5} can be achieved with a filling factor as small as 0.004. The temperature required is 3.2×10^5 K. But, with the same assumptions, a filling factor, f, as high as 0.6 can be inferred just by raising the assumed temperature to about 10^6 K.

Jenkins tried two methods for restricting the estimated hot gas filling factor. In one, he sought a possible anticorrelation between O^{+5} and reddening, under the notion that O^{+5}-bearing gas might noticeably displace denser gas. From the weak to nonexistent effect found in the data, he concluded that f was less than 20%, or that the hot gas does not effectively displace the material responsible for the reddening (i.e., it displaces only very diffuse intercloud gas).

His other method assumed $p/k = 10^4$ K cm^{-3}, a power-law temperature distribution function, steady state or time-dependent ionization, and attempted to fit the mean density of O^{+5}, the widths of the narrowest lines, and the N^{+4} to O^{+5} ratio, while not overproducing the soft X-ray background. Even this effort yields only very weak limiting information because the O^{+5} ion poorly samples gas hotter than a million degrees, while the filling factor for acceptable power laws tends to concentrate there. For example, Jenkins estimated the lower limit in f to be 0.18, with a power-law index of 0.5 and an upper temperature bound of $T_2 = 2 \times 10^6$ K. There is, however, no information to indicate that T_2 should be nearly that high, now that it appears that the soft X-ray background is largely a local phenomenon not directly related to the interstellar O^{+5}. Lowering T_2 to 10^6 K, reduces the estimate to 0.06. Using our values of n_o decreases this estimate even further.

This problem can also be approached via methods based on estimates of the sizes of O^{+5}-bearing gas regions and of the mean free path between line-of-sight encounters with them in the ISM. For roughly spherical regions, the filling factor is given by

$$f \cong d/\lambda\,,$$

where d is the mean region scale and λ the encounter mean free path. Thus, should one be disposed to believe that the O^{+5} is in regions of cloud evaporation, with typical scale of $d \sim 10$ pc, then our result from § 4 that $\lambda \sim 450$–1300 pc suggests that $f \sim 0.008$–0.025. If, on the other hand, one presumes the O^{+5} to lie in superbubbles with typical scale of 100 pc, then the filling factor for those bubbles would be $f \sim 0.08$–0.25. (The filling factor for the gas actually bearing the O^{+5} could be considerably smaller if much of the bubble volume is too hot for O^{+5}.)

For the most part, the O^{+5} data must be compared with specific models for its origin, constraining them directly rather than through a more generic "filling factor" estimator. We do this in § 7.2.

7. DISCUSSION

7.1. *Local Bubble*

Our analysis provides a realistic estimate of the local O^{+5} component for comparison with model predictions. The mean value lies in the range 1.2–2.0 $\times 10^{13}$ cm^{-2}, a span that includes the only strong peak in the column density histogram (Fig. 1). That histogram also shows very few stars with column densities around 2.3×10^{13} cm^{-2}, providing a natural cutoff for sight lines that probably have only local O^{+5}. Hereafter, the sight lines with detected column densities less than 2.0×10^{13} cm^{-2} will be referred to as the low column density or LCD subset.

One caveat deserving discussion (Jenkins 1984) is the possibility that the local component is actually local to the individual stars, rather than to the Sun. Both the absence of O^{+5} toward very nearby stars and the fact that few LCD targets are powerful O stars speak against this possibility. But B stars may have devices unknown to us and the nearby paucity might be an oddity, related somehow to the abnormally low density in the local cavity. To test the circumstellar hypothesis, Jenkins (1978b) examined the entire data set, but found little evidence that O^{+5} is associated with the target stars. One criterion was based on the expectation that circumstellar O^{+5} would be due to wind cavities and that the column density would decrease with increasing velocity of the star toward us through the surrounding medium. He thus searched for a positive correlation between $N(O^{+5})$ and $v_{\rm star} - v_{\rm gal}$ where $v_{\rm gal}$ is the Galatic rotation velocity at the location of the star. We have performed this same test for stars with $N < 2 \times 10^{13}$ cm^{-2}, finding a very weak *negative* correlation. We have also explored two other possibilities, that the LCD stars may have O^{+5} velocities related either to the stellar velocities (they do not) or to the interstellar gas (they do not). Thus, we find no evidence that the LCD O^{+5} is associated with circumstellar gas.

7.1.1. *Data*

If the 1–2.0 $\times 10^{13}$ cm^{-2} column densities are related to the Local Bubble, rather than to the stars, then the velocity field sampled by those absorption features should provide useful information on the kinematics of the Local Bubble boundary. We have therefore examined the velocity field of the 27 LCD sight lines for evidence of bubble expansion or contraction,

translation, turbulence, shear, other patterns of deformation, and correlation with stellar velocity.

Three of the sight lines (ϵ Per, HD 52918, and δ Cru) have only weak features ($\lesssim 10^{13}$ cm^{-2}) at about +50 km s^{-1}. These three sight lines are short, close to the Galactic plane, and in widely differing directions. They suggest that the Local Bubble contains a radial flow field at 50 km s^{-1}, carrying 10^{13} cm^{-2} O^{+5} ions. The rms velocity spread, $[\int (v - \bar{v})^2 \tau\, dv / \int \tau\, dv]^{1/2}$, is about 14 km s^{-1}. This weak feature could be hiding in the wings of many other profiles and appears to be present as a secondary peak in ν Cen. On the other hand, the data quality is such that these velocities may be incorrect.

The velocity data on the remaining 24 sight lines is highly variable in quality, with differences in the mean velocities measured in the two lines of the doublet varying between 0.4 and 17.7 km s^{-1}—omitting HD 64740 for which it is quoted to be even larger but appears uncertain. In addition, the sky sampling is very incomplete.

We have found no systematic trend for either expansion or contraction; the average and median velocities are very near zero. The column density weighted rms velocity, however, is 12 km s^{-1}. For comparison, the instrumental resolution is 14.5 km s^{-1} (Rogerson et al. 1973).

Our attempt to measure a dipole moment in the radial velocity distribution, due to a possible translation vector for the local ISM and the bubble boundary, yielded only insignificant results. Thus, our local O^{+5} analysis could find neither the Crutcher vector ($v \simeq -28$ km s^{-1}, $l \simeq 25°$, $b \simeq 10°$ heliocentric or $v \simeq -15$, $l \simeq 345$, $b \simeq -10°$, LSR; Crutcher 1982), representing the generally nearby ISM, nor the interstellar wind vector (blowing from $l \simeq 5°$, $b \simeq 19°$, with a heliocentric velocity of $\sim$25 km s^{-1}; Weller & Meier 1979, 1980) representing the local flow of interstellar material through the solar system.

We examined the data for the velocity shear pattern representative of differential rotation. For those sight lines showing O^{+5} above what is expected from the Local Bubble alone, the pattern matches that expected when the absorbing gas is assumed to be halfway between the Sun and the target star. There is considerable scatter, but a good correlation. Many of the LCD stars, however, are so nearby that differential rotation should be negligible compared to the measured dispersion of velocity centroids, and we do not find a statistically significant positive correlation.

The radial velocities for the LCD sight lines do, however, exhibit patterns, though they cannot be generalized without measurements in more directions. For the most part, the local hot gas in the Scorpius and Orion directions is approaching us, while in Cygnus and Perseus it is receding. Centaurus has both approaching and receding sections. A number of sight lines show velocities roughly similar to the Crutcher vector, though they seem to be restricted to fairly low latitudes (below $b = +12°$ in Scorpius, and north of Orion in the anticenter direction). Furthermore, the two high northern latitude ($b > 30°$) LCD stars have long sight lines, somewhat similar directions, and the same O^{+5} velocity of −15 km s^{-1}. Perhaps, in this measure as in others (e.g., Danly 1989), the northern sky is falling.

The local sight lines exhibit a wide range of line widths. The lowest values may provide some insight into the physical conditions in their source regions, but since they may be influenced by accidental downward fluctuations due to observational errors (Jenkins 1978b), a reasonable quantity for comparison is the lowest spread occurring consistently in both the 1032 and 1038 Å data for a sight line. For this case the corresponding rms velocity spreads are 11.4–12.1 km s^{-1}, implying $T \simeq 2.5$–2.8×10^5 K. For comparison, when the −50 km s^{-1} sight lines are excluded, the median spread for the 1032 Å line is 16.7 km s^{-1}. The greater widths could derive from turbulence in the hot Local Bubble, from velocity gradients across the regions, or from multiple components (e.g., the Local Bubble outer wall and the Local Bubble interface with the Local Cloud, or other such nearly interfaces).

7.1.2. *Models*

These characteristics can be compared with four existing models for the origin of O^{+5} in the local environment, all of which have been based on the presumption that the soft X-ray background arises from roughly 10^6 K gas in a Local Bubble, surrounding the solar location out to $\sim$100 pc. The locations are the following:

1. The evaporative transition layer between the Local Cloud and the hot gas of the Local Bubble (or between other cool inclusions and the hot gas)
2. The hot gas of the Local Bubble itself
3. The boundary of the Local Bubble, modeled as the remnant of a fairly recent supernova (age $\sim 10^5$ years) and
4. The outer layers of the Local Bubble, modeled as the quiescent residual of a much older explosion.

Slavin's (1989) model for O VI on the boundary of the Local Cloud assumed nonequilibrium ionization in a steady, spherical, evaporative flow. The cloud radius was assumed to be 3 pc and the flow followed to 30 pc (therefore including a substantial fraction of the Local Bubble in the column density integral). Depending on assumptions about the magnetic field, he found O^{+5} column densities in the range 0.7–1.4 $\times 10^{13}$ cm^{-2}, with an average radial velocity of 0.6–13.1 km s^{-1} and line widths of 15.8–19.1 km s^{-1}.

None of our LCD sight lines show O VI profiles precisely within these parameter ranges. Some have higher column densities; some have narrower profiles, and some have negative radial velocities. Furthermore, three stars, that are probably outside the Local Cloud but closer than the Local Bubble boundary, have very little O^{+5}. The single counterexample is α Eri. Its profile has a column density of 1.1×10^{13} cm^{-2}, a radial velocity of 6.9 km s^{-1}, and a rms velocity spread of 21.3 km s^{-1}, in a sight line of only 26 pc. Apart from the line width (which could have been broadened by turbulence, or in error), this could be the best candidate for observing evaporation flow on the boundary of the Local Cloud. The message of other local sight lines appears to be that such evaporation does not occur uniformly over the cloud at the rate implied for the α Eri direction.

There are probably other low-density clouds within the Local Bubble, additional examples of Local Fluff (e.g., see Cox & Reynolds 1987). Evaporative flow from the near sides of such clouds would be seen by us with negative radial velocities, added to the cloud velocities. Similarly, the velocity of the Local Cloud itself is sufficiently great that even evaporative flow from it could appear at a slightly negative radial velocity in directions generally toward the Galactic center. As a consequence, despite the existence of negative radial velocities, the local O^{+5} could be contributed primarily by boundaries of evaporating clouds within the hot Local Bubble. The strongest observational reasons for supposing otherwise are that few of

the stars within the first 100 pc have O^{+5} in front of them, and some line profiles are narrower (12 km s^{-1}) than can easily be provided by evaporative boundaries of sufficient column density (see Borkowski, Balbus, & Fristrom 1990). (This may not be true of the later *condensation* stage.)

The possibility that the 10^6 K gas surrounding the solar location might contribute directly to the observed O^{+5} population was proposed by Cox & Smith (1974). They estimated the O^{+5} density to be 10^{-8} cm^{-3}, providing a column density of 0.3×10^{13} cm^{-2} per 100 pc. At slightly lower temperatures, the O^{+5} concentration is generally much higher, however, suggesting that cooler boundary layers might dominate the observations. Although it would be confirming to find broad weak components consistent with the 10^6 K gas thought to be filling the Local Bubble, the existing observational material is inadequate for these purposes.

Various ways in which the Local Cavity may have come into being, and ways in which a portion of it, the Local Bubble, may have been heated to 10^6 K were discussed by Cox & Reynolds (1987). Among those is the possibility that the Local Cavity is a fairly ordinary part of the interstellar medium in which intercloud densities of order 10^{-2} cm^{-3} are the norm. The Local Bubble can then be modeled as the remnant of a single supernova explosion in low ambient density (e.g., Cox & Anderson 1982; Arnaud, Rothenflug, & Rocchia 1984). A related possibility is that the cavity was formed in a higher density intercloud component, perhaps by a sequence of earlier explosions, and then the central parts reheated by a single recent supernova (e.g., Edgar 1986). In both of these situations, it was assumed that the outer boundary of the hot gas is a fast ($\simeq 260$ km s^{-1}) shock presently heating material to 10^6 K. With a shock radius of about 100 pc, an age of approximately $0.4R/v_s \simeq 1.5 \times 10^5$ yr is implied. Though controversial (Frisch 1993), recent identification of Geminga as the stellar remnant of such an explosion, possibly inside the Local Bubble approximately 3×10^5 years ago (Gehrels & Chen 1993), lends further credence to models of this type. Both Cox & Anderson (1982) and Edgar (1986) found model parameters that led to the correct X-ray surface brightness and X-ray band ratio, at internal pressures that are roughly comparable to ambient. Edgar also showed that it was possible with such models to have, as observed, a lower X-ray brightness in directions for which more external material was encountered.

The O^{+5} column densities in such models were shown by Cox & Anderson to be sensitive primarily to only one parameter, the preshock ionization state. Edgar's work confirmed this for explosions in cavities. Unless the preshock gas was already ionized beyond O^{+5}, the predicted column densities were high, about 4×10^{13} cm^{-2}. Most of the O^{+5} is just inside the shock front, and should be moving outward at about 3/4 of the shock velocity, 200 km s^{-1} (or somewhat less as the compression is reduced by having a significant ambient pressure). It should also have a line width corresponding to at least 10^6 K. This column density is far higher than the 1.6×10^{13} cm^{-2} of local O^{+5} which we find from the existing data. On the other hand, the expected velocity is also well outside the range actually measured by *Copernicus* in most cases. It is just possible that when a broader velocity range is explored, this fast O VI will be found.

Another class of models beginning to be explored assumes that both cavity formation and the reheating of the center occurred long ago so that there is no longer a fast shock wave at the bubble boundary. Results from the first of this class were presented by Edgar & Cox (1993). They assumed that a single large explosion both created the cavity and left the central bubble hot. For runs that succeeded in generating the cavity and producing about the right C band (1/4 keV) X-ray surface brightness, the O VI column densities were roughly 1–2.5×10^{13} cm^{-2}, similar to our range of Local Bubble column densities. Furthermore, when this column density is added to that of Slavin's Local Cloud boundary (without double counting the first 30 pc of the Local Bubble), the result agrees with the range found by our analysis. Edgar & Cox did not present information on the anticipated velocity or velocity width, but in this type of model, both could be small. The mean velocities can be of either sign, depending on whether the bubble is still expanding or has begun contraction, a distinction that may vary gradually with direction. As discussed by Slavin & Cox (1992), boundaries at which cooling and condensation are occurring will have O^{+5} at lower temperatures than equilibrium or evaporation boundaries and will therefore have narrower lines. Thus, the initial foray into this class of models yields characteristics that are consistent with our Local O^{+5} results. The models, however, have various other difficulties (requiring too large a confining pressure, getting the wrong X-ray B/C band ratio, and ignoring the fact that the dust destruction timescale is very long), and require much further development.

As a final remark, we note that information on the anticipated O^{+5} *emission* is published for only a few of these models. Such information would provide an interesting point of comparison with future diffuse measurements in the EUV.

7.2. *Distant Features*

For years, Jenkins's estimated mean O^{+5} column density per hot feature, N_o, and mean planar volume density, have been benchmarks for judging ISM models. After updating the analysis by including the Local Cloud and Bubble and making a small mathematical improvement, we found $\overline{N_o}$ to be $2–7 \times 10^{13}$ cm^{-2}, which is 2–7 times larger than Jenkins's value. We also found $\hat{n_o}$ to be $1.3–2.1 \times 10^{-8}$ cm^{-3}, which is somewhat smaller. Therefore, new insights may be found by comparing our results with models, such as those for old supernova remnants, fountains, and wind-blown bubbles.

The most frequently discussed possible source of this high ion is the conductive interfaces on clouds embedded in very hot intercloud gas. This interpretation was initially advanced by McKee & Ostriker (1977) and appeared to have observational support in Cowie et al. (1979), who found that the O^{+5} velocities and widths may be related to a subset of the features found in lower ions, particularly Si^{+2}. Böhringer & Hartquist (1987) calculated the O^{+5} column density in a single conductive interface between spherical clouds and hot ($T = 0.5–1 \times 10^6$ K), unmagnetized gas to be $0.3–2.0 \times 10^{13}$ cm^{-2}, depending upon the specific model parameters. Because these represent the perpendicular column density through a single interface, these column densities should be multiplied by a geometrical factor of ≥ 2 (Spitzer 1990), for comparison with cloud surfaces. Borkowski et al. (1990) calculated the O^{+5} column density for magnetized planar conductive fronts. Their column densities are dependent on initial magnetic field inclination, with the greatest being only about 1×10^{13} cm^{-2} for a single interface. Of course, the collection of existing and conceivable conductive interface models is extraordinarily rich, with various ambient conditions, possible magnetic effects, and differing geometries.

Such interfaces may be able to contribute column densities

within our range, but the whole idea that the observed O^{+5} traces cloud surfaces is brought into question by the fact that the number of clouds on a line of sight far exceeds the number of O^{+5} features. This inconsistency implies that even if the clouds are sheetlike, at most a minority of their surfaces supply large O^{+5} column densities. For other cloud geometries, the thickness of the evaporation layer enhances the probability of encounter and the fraction of clouds with such layers must be much smaller yet.[9] As a result, if hot gas is prevalent, clouds with large O^{+5} column densities must be somehow exceptional. Alternatively the initial assumption of a pervasive distribution of hot intercloud gas may be incorrect and the O^{+5} located in active disturbances.

Edgar & Chevalier (1986) have calculated the expected O^{+5} column density due to fountains of supernova heated gas for a sight line through the Galactic disk and halo. They assumed that the initially very hot gas cooled steadily with negligible heat conduction, and considered cases that were isobaric, isochoric, or isobaric with a transition to isochoric. With 4 $M_\odot$ yr^{-1} heated above a critical temperature on each side of the plane and an initial hydrogen density, $n_{H,o}$, of 10^{-3} cm^{-3}, they found the expected column density for O^{+5} to be about 6.0×10^{14} cm^{-2}. Shapiro & Benjamin (1992) have also calculated the O^{+5} column density associated with Galactic fountains. Their work, which included self-ionization and scaling to the observed C^{+3} column density, yielded O^{+5} column densities between 1.9 and 3.0×10^{14} cm^{-2} for $n_{H,o} D_o \geq 0.40$ pc cm^{-3}, where D_o is the size of the cooling region. A comparison with our results is limited because the O VI data apply to relatively low latitudes ($\overline{|z|} = 425$ pc for the observed stars). With a scale height of 3000 pc and $\hat{n_o} = 1.6 \times 10^{-8}$ cm^{-3}, however, the one-sided column density out of the disk would be only about 1.5×10^{14} cm^{-2}, about a fourth of Edgar & Chevalier's result and below the low end of Shapiro and Benjamin's range. Edelstein & Bowyer's (1993) recent relatively high-latitude O^{+5} emission upper limit is also lower than Edgar & Chevalier's emission prediction by about a factor of 3 when the prediction is scaled to match the observed C^{+3} emission, while the high column density to 3C 273 (Davidsen 1993) appears to push in the opposite direction.

These modelers assumed laminar flow in their one-dimensional models. Work on turbulent mixing layers by Slavin, Shull, & Begelman (1993), however, shows that such regions may contribute to the O^{+5} column density on some lines of sight and increase variation in neighboring directions.

Material heated by magnetic reconnection in microflares, as discussed by Raymond (1992) could be an even more important source of high-stage ions at larger $|z|$.

Slavin & Cox (1992, 1993) have investigated the long-term evolution of a supernova remnant in a warm intercloud environment. (They simulated a spherically symmetric remnant evolving in a homogeneous ambient medium with a temperature of 10^4 K, density of 0.2 cm^{-3}, and nonthermal pressure equivalent to that of a 5 μG magnetic field.) They found a very long-lived bubble of O^{+5} bearing gas, well after dispersal of the remnant's shell. They also found that bubbles are able to make a substantial contribution to the observed mean O^{+5} density without requiring large porosity for the medium. The anticipated column densities varied somewhat with explosion energy, ambient density, and pressure, as well as the bubble age and impact parameter. The expected range is roughly 2–9 $\times 10^{13}$ cm^{-2}, with the larger values being considerably less common. The most probable value is about 4.7×10^{13} cm^{-2}. While at odds with Jenkins's original analysis, this model appears to be consistent with our results.

In this model, much of the O^{+5} is found near the outer edge of the bubble in a condensation front. Because the O^{+5} velocity characteristics are not that dissimilar from those in the surrounding ISM (the former shell material) and the low-stage ions therein, the relationship between O^{+5} and Si^{+2} velocities should be fully consistent with the Cowie et al. (1979) correlation. To carry this further, the finding that the O^{+5} is correlated with only a subset of the Si^{+2} can easily be understood if hot gas fills a small fraction of the total volume, because one would expect fewer regions at the very high temperatures that produce O^{+5} than at conditions required to produce Si^{+2}.

Another potential contribution is O^{+5} in hot stellar wind bubbles encountered coincidentally along the line of sight. According to Weaver et al. (1977), a radial path through one side of a typical million year old wind bubble in a 1 cm^{-3} ambient medium has an O^{+5} column density of 2.3×10^{13} cm^{-2}. The value changes very little with age and depends only weakly on the assumed wind luminosity. For comparison with our results, it should be doubled for the two sides and the considerable dependence on impact parameter recognized. The range and variability of the column densities is then consistent with our results. A complication is that many of the stronger wind-producing stars are located within clusters that may make the collective superbubble a more relevant entity for modeling and comparison. Orion, the Gum Nebula, and the Sco-Cen association are candidate sites for such collective bubbles affecting the *Copernicus* O^{+5} observations.

Apparently, wind and relic SNR bubbles can be expected individually to harbor similar quantities of O^{+5}. The SNR bubbles should be considerably more common in the general ISM and probably contribute most to the mean interstellar density of this ion. On the other hand, quite a few stars in this data set lie within or beyond OB associations, complicating the sampling.

8. CONCLUSIONS

The implications of the *Copernicus* O^{+5} data have changed substantially as a consequence of the work presented in this paper. Unless the existing data form a very unrepresentative sample, we can no longer think of the O^{+5} along a sight line as being encountered commonly, in small quantities, perhaps in the surfaces of interstellar clouds immersed in a coronal intercloud component. Nor can we ignore the contribution from the Local Bubble.

There is a major local component.—O^{+5} surrounding the solar location was expected from soft X-ray evidence. The results of our statistical analysis, the details of the column density distribution for nearby stars, and a single strong peak in the histogram of column densities are all in accord with this expectation. The most probable column density is 1.6×10^{13} cm^{-2}, the range from 1 to 2.2×10^{13} cm^{-2}. More than a third of the *Copernicus* stars show only this local component.

It is not in vigorous motion.—The velocity data from this low column density subset of the profiles, presumably indicative of Local Bubble kinematics, have a low value of column density weighted rms velocity (12 km s^{-1}), modest line widths, and some coherence on the scale of constellations. They also show

[9] For example, the original McKee & Ostriker model, formulated prior to Jenkins's (1978b) analysis, had a cold cloud encounter rate of 6 per kpc, but a cloud envelope encounter rate of about 80 per kpc! Our result is that the correct answer for O^{+5} is 1–2 per kpc.

no apparent expansion or contraction and no significant bulk flow. Another intriguing aspect is that three low latitude stars in widely differing directions seem to show a weak feature at $+50$ km s^{-1}.

There are several potential sources.—A portion of the local component may be in evaporation boundaries on very diffuse clouds within the hot Local Bubble (on the Local Cloud in particular) and in the hot cavity itself, but the dominant contribution appears to be at the bubble's outer surface. When the Local Bubble is modeled as a young ($\sim 10^5$ yr old) SNR, a large O^{+5} column density is expected from the region just interior to the shock; its expected radial velocity, however, is outside the range observed by *Copernicus* in most cases. The applicability of such a model cannot be ruled out, but it would not provide the low-velocity O^{+5} actually observed. Quiescent older bubbles seem to have greater success explaining the existing data, but their modeling is only in its infancy.

Beyond the Local Bubble, O^{+5} regions are few and far between.—Column densities higher than those attributed to the local component are rare in stars nearer than about 400 pc. In accordance, our statistical analysis yields a much larger mean free path, λ, between such encounters (450–1100 pc) than the 165 pc found in Jenkins's earlier work (1978b). Thus we find a smaller number of encounters per kpc (1–2 rather than 6).

The 29 CMa and τ CMa data provide a good example of the long distances possible between encounters with hot features. These lines of sight are only 25′ apart and, according to Jenkins (1987a), have nearly identical O VI profiles. They apparently traverse exactly the same hot gas regions, even though the estimated distance for 29 CMa is about 1000 pc greater. With our large λ, a 1000 pc path with no encounters is not surprising, but with Jenkins's λ of 165 pc, it is extremely unlikely. (There is, however, some uncertainty about the distance between these two stars, as discussed in Jenkins 1978b.)

On the other hand, O^{+5} column densities do sometimes vary rapidly from one star to the next, hinting that individual contributors must be common enough for different ones to be sampled by proximate stars. For example, Jenkins called attention to Orion, where neighboring stars do have very different column densities. Perhaps, when the *ROSAT* data on this region become more widely available, it will be possible to see whether much of the O^{+5} along those sight lines might accrue from the complicated boundary of the Orion-Eridanus superbubble, making the observed column density depend sensitively on the boundary configuration and the stellar locations relative to it. By analogy with the filamentary optical emission of the Cygnus Loop, it should not be surprising that very different column densities can arise from the complexity of a single O^{+5}-bearing surface.

Typical O^{+5} regions in the ISM have large column densities.—Our statistical analysis found that the large mean free path is accompanied by a mean column density per feature of $2\text{–}7 \times 10^{13}$ cm^{-2} and a mean density $\widehat{n_o} = \overline{N_o}/\lambda$ of $1.3\text{–}2.1 \times 10^{-8}$ cm^{-3}.

The large column densities are not a problem for models.—Column densities within the indicated range have been found by modelers of evaporating interstellar clouds, very old SNR bubbles, and stellar wind bubbles. The SNR bubble possibility has been discussed extensively by Slavin & Cox (1992, 1993). Within the uncertainties, it can provide the right size features and the right mean free path (and therefore mean density). The required remnant population evolves in the warm intercloud medium and occupies less than 10% of interstellar space. The bubbles blown by stellar winds could individually be similar to those of SNRs, but should be considerably less common. Superbubbles, however, offer another source site, for which there is presently no adequate census.

The large mean free path creates a serious problem for cloud evaporation models.—Clouds are much more commonly encountered than are O^{+5} regions. For that reason, if the O^{+5} is in interfaces between cold clouds and pervasive hot gas, suitable interfaces exist on only a small fraction of the clouds. Those clouds must somehow be quite unusual. Another possibility is that hot gas is not prevalent and individual O^{+5} features are associated with active events (SNRs, superbubbles).

Several important issues cannot be adequately addressed with the existing O^{+5} data.—It is not possible to define a scale height for the O^{+5} gas, determine whether there is a $|z|$ dependence to the characteristic feature properties, search for the high-$|z|$ onset of a fountain or chromospheric contribution, determine whether there is a significant gradient with galactocentric radius, set a meaningful, model-independent, upper bound on the volume fraction of O^{+5}-bearing gas, or discover whether a potential high-velocity (~ 200 km s^{-1}) component is present in the local interstellar medium.

Dedicated efforts can be expected to provide better absorption-line data, diffuse emission-line measurements, images, and velocity-resolved maps. We may see measurements of the broad, but weak, absorption from 10^6 K gas within the Local Bubble, exploration of the validity of the mysterious $+50$ km s^{-1} local component, a definitive search for a $+200$ km s^{-1} component indicative of a young blast wave in the Local Bubble, improved line profiles that will test the statistical results and can be compared with N^{+4} and C^{+3} data for the same stars, and measurements that better sample the Local Bubble kinematics, the halo distribution, and the radial gradient. Diffuse emission studies will provide important constraints on potential sources within and beyond the Local Bubble, especially the Local Bubble boundary, the SNR bubble population, and a Galactic fountain. Finally, our grossly oversimplified conceptions of the diffuse ISM will be shattered by orbiting instrumentation able to form large-scale images. A radial velocity-resolved map of the far-ultraviolet line emission will provide the fullest possible information about the distribution and kinematics of the hot gas and its relationship to the cooler components of the medium. Our present expectation is that the interstellar structures glowing in O VI will be highly filamentary, highlighting the hot gas boundaries within and at the edges of relic SNRs and superbubbles, possibly also tracing the surfaces of clouds immersed within the Local Bubble. Regions in which there are strong gradients in the soft X-ray background, or in H I, provide good candidate directions. Canis Major could be exciting. These expectations, however, may pale before the surprises in store for us when the observations are finally made.

The authors would like to thank Barbara Armstrong for providing a portion of the simulated data sets, Edward Jenkins for an extremely helpful referee's report that grew into many useful discussions, and Ron Reynolds, Chuck Joseph, and Dick Edgar for helpful comments on the manuscript. This work was supported by the National Aeronautics and Space Administration under grants NAG5-629 and NAGW-2532.

REFERENCES

Armstrong, B. 1992, private communication
Arnaud, M., Rothenflug, R., & Rocchia, R. 1984, in IAU Colloq. 81, Local Interstellar Medium, ed. Y. Kondo, F. C. Bruhweiler, & B. D. Savage (NASA CP-2345), 301
Bertaux, J. L., Lallement, R., Kurt, V. G., & Mironova, E. N. 1985, A&A, 150, 1
Böhringer, H., & Hartquist, T. W. 1987, MNRAS, 228, 915
Borkowski, K. J., Balbus, S. A., & Fristrom, C. C. 1990, ApJ, 355, 501
Chassefière, E., Bertaux, J. L., Lallement, R., & Kurt, V. G. 1986, A&A, 160, 229
Cowie, L. L., Jenkins, E. B., Songaila, A., & York, D. G. 1979, ApJ, 232, 467
Cox, D. P., & Anderson, P. R. 1982, ApJ, 253, 268
Cox, D. P., & Reynolds, R. J. 1987, ARA&A, 25, 303
Cox, D. P., & Smith, B. W. 1974, ApJ, 189, L105
Crutcher, R. M. 1982, ApJ, 254, 82
Danley, L. 1989, ApJ, 342, 785
Davidsen, A. F. 1993, Science, 259, 327
Edelstein, J., & Bowyer, S. 1993, Adv. Space Res., 13(12), 307
Edgar, R. J. 1986, ApJ, 308, 389
Edgar, R. J., & Chevalier, R. A. 1986, ApJ, 310, L27
Edgar, R. J., & Cox, D. P. 1993, ApJ, 413, 190
Frisch, P. 1993, Nature, 364, 395
Gehrels, N., & Chen, W. 1993, Nature, 361, 706
Jenkins, E. B. 1978a, ApJ, 219, 845
———. 1978b, ApJ, 220, 107
Jenkins, E. B. 1978c, Comm. Astrophys., 7, 121
———. 1984, in IAU Colloq. 81, Local Interstellar Medium, ed. Y. Kondo, F. C. Bruhweiler, & B. D. Savage (NASA CP-2345), 155
McKee, C. F., & Ostriker, J. P. 1977, ApJ, 218, 148
Raymond, J. C. 1992, ApJ, 384, 502
Rogerson, J. B. Spitzer, L., Drake, J. F., Dressler, K., Jenkins, E. B., Morton, D. C., & York, D. G. 1973, ApJ, 181, L97
Savage, B. D., et al. 1993, ApJ, 413, 116
Savage, B. D., & Massa, D. 1987, ApJ, 314, 380
Sciama, D. W. 1972, Nature, 240, 456
Shapiro, P. R., & Benjamin, R. A. 1992, in Star Formation, Galaxies and the Interstellar Media, ed. J. Franco, F. Ferrini, & G. Tenorio-Tagle (Cambridge: Cambridge Univ. Press), 275
Slavin, J. D. 1989, ApJ, 346, 718
Slavin, J. D., & Cox, D. P. 1992, ApJ, 392, 131
———. 1993, ApJ, 417, 187
Slavin, J. D., Shull, J. M., & Begelman, M. C. 1993, ApJ, 407, 83
Snowden, S. L., Cox, D. P., McCammon, D., & Sanders, W. T. 1990, ApJ, 354, 211
Spitzer, L. 1990, ARA&A, 28, 71
Weaver, R., McCray, R., Castor, J., Shapiro, P., & Moore, R. 1977, ApJ, 218, 377
Weller, C. S., & Meier, R. R. 1979, ApJ, 227, 816
———. 1980, BAAS, 11, 684